

1 Poly(2-isopropyl-2-oxazoline)-*b*-poly(lactide) (PiPOx-*b*-PLA) 2 Nanoparticles in Water: Interblock van der Waals Attraction 3 Opposes Amphiphilic Phase Separation

4 Fabian Pooch,[†] Marjolein Sliepen,[†] Kenneth D. Knudsen,[‡] Bo Nyström,[§] Heikki Tenhu,[†]
5 and Françoise M. Winnik^{*,†,||}

6 [†]Department of Chemistry, University of Helsinki, P.O. Box 55, Helsinki 00014, Finland

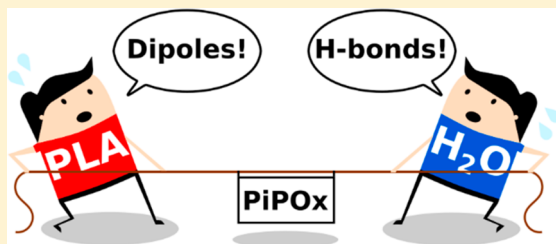
7 [‡]Department of Physics, Institute for Energy Technology, P.O. Box 40, N-2027 Kjeller, Norway

8 [§]Department of Chemistry, University of Oslo, P.O. Box 1033, Blindern, N-0315 Oslo, Norway

9 ^{||}International Center for Materials Nanoarchitectonics, National Institute for Materials Science, 1-1 Namiki, Tsukuba 305-0044,
10 Japan

11 **S** Supporting Information

12 **ABSTRACT:** Poly(2-isopropyl-2-oxazoline)-*b*-poly(lactide) (PiPOx-
13 *b*-PLA) diblock copolymers comprise two miscible blocks: the
14 hydrophilic and thermosensitive PiPOx and the hydrophobic PLA, a
15 biocompatible and biodegradable polyester. They self-assemble in
16 water, forming stable dispersions of nanoparticles with hydrodynamic
17 radii (R_h) ranging from ~ 18 to 60 nm, depending on their molar mass,
18 the relative size of the two blocks, and the configuration of the lactide
19 unit. Evidence from ¹H nuclear magnetic resonance spectroscopy, light
20 scattering, small-angle neutron scattering, and cryo-transmission
21 electron microscopy indicates that the nanoparticles do not adopt the typical core-shell morphology. Aqueous nanoparticle
22 dispersions heated from 20 to 80 °C were monitored by turbidimetry and microcalorimetry. Nanoparticles of copolymers
23 containing a poly(DL-lactide) block coagulated irreversibly upon heating to 50 °C, forming particles of various shapes ($R_h \sim$
24 200–500 nm). Dispersions of PiPOx-*b*-poly(L-lactide) coagulated to a lesser extent or remained stable upon heating. From the
25 entire experimental evidence, we conclude that PiPOx-*b*-PLA nanoparticles consist of a core of PLA/PiPOx chains associated
26 via dipole-dipole interactions of the PLA and PiPOx carbonyl groups. The core is surrounded by tethered PiPOx loops and
27 tails responsible for the colloidal stability of the nanoparticles in water. While the core of all nanoparticles studied contains
28 associated PiPOx and PLA blocks, fine details of the nanoparticles morphology vary predictably with the size and composition
29 of the copolymers, yielding particles of distinctive thermosensitivity in aqueous dispersions.



30 **■** INTRODUCTION

31 In selective solvents, diblock copolymers (BCPs) tend to self-
32 assemble into core-corona structures above their critical
33 micelle concentration (cmc),¹ as it is the case for surfactants,
34 their low molecular weight counterparts. The BCP micelle core
35 is formed by the solvophobic blocks, while the soluble blocks
36 in the corona provide colloidal stability to the micelle. The
37 thermodynamically favored micelle morphology depends on
38 the volume fraction of the solvophilic and solvophobic blocks,
39 which is related to the molecular properties of the two blocks,
40 namely their molar mass and chemical composition. It is
41 affected also by the quality of the solvent for the solvophilic
42 block and by the attraction of the two blocks toward each
43 other.² When a solvent-selective BCP comprises two blocks
44 miscible in the bulk phase, the attraction between the two
45 blocks becomes an important parameter to consider when
46 assessing its assembly in a selective solvent. We recently
47 reported that poly(L-lactide)-*b*-poly(2-isopropyl-2-oxazoline)
48 (PiPOx-*b*-PLLA) BCPs are miscible in the bulk.³ Dipolar

interactions of the carbonyl groups of the PiPOx and PLA 49
blocks are responsible for the miscibility, as confirmed 50
experimentally in the FTIR spectra of PiPOx-*b*-PLLA, which 51
presents shifts of the PiPOx carbonyl-stretching vibrations as a 52
function of the PLLA content. The close values of the 53
solubility parameters of PiPOx and PLA (δ_{PiPOx} : 24.0 J^{0.5}/
cm^{1.5}; δ_{PLA} : 22.7 J^{0.5}/cm^{1.5}) calculated by the method of 54
Fedors⁴ support the experimental observations. 55
56

PiPOx is a semicrystalline polymer soluble in polar organic 57
solvents and in cold water. Its aqueous solutions undergo a 58
phase transition upon heating, yielding a phase-separated 59
turbid suspension from which PiPOx eventually crystallizes in 60
the form of fibrillar nanostructures.⁵ The phase transition 61
temperature of aqueous PiPOx solutions markedly depends on 62
the polymer molecular weight. The cloud point temperature 63

Received: November 30, 2018

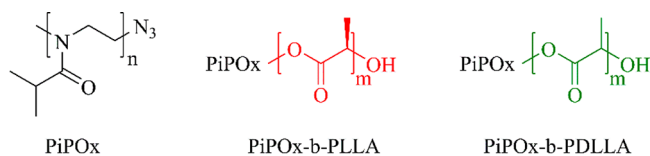
Revised: January 16, 2019

64 (T_{CP}) of PiPOx in water (1 g/L) decreases from 73 to 36 °C as
 65 the PiPOx molar mass (M_n) increases from 1.9 to 16.7 kg/
 66 mol.^{6,7} Oligo-PiPOx samples consisting of six repeating units
 67 or fewer ($M_n < 0.7$ kg/mol) remain soluble in water beyond 80
 68 °C.⁸ Previously reported diblock copolymers consisting of a
 69 PiPOx block and a water-insoluble block were shown to
 70 associate in water in the form of core/corona nanoparticles
 71 with a core containing the hydrophobic blocks and a corona
 72 consisting of hydrated PiPOx chains. Upon heating the BCPs
 73 dispersions in water beyond their phase-transition temperature,
 74 a sharp increase of turbidity occurred, reflecting the
 75 cooperative dehydration of the PiPOx blocks and subsequent
 76 interparticle aggregation. Examples of hydrophobic blocks
 77 employed include poly(ethylene), poly(2-(4-*tert*-
 78 butoxycarbonyl)amino)butyl-2-oxazoline), and poly-
 79 (ferrocenyldimethylsilane).^{9,10} Stoichiometric mixtures in
 80 water of two oppositely charged diblock ionomers, such as
 81 the PiPOx-*b*-poly(L-lysine)/PiPOx-*b*-poly(aspartic acid) pair,
 82 also assemble in water, forming core–corona polyion complex
 83 (PIC) micelles first reported by Kataoka.¹¹ Dihydrophilic
 84 block copolymers are also of interest, in which the PiPOx block
 85 is linked to another water-soluble block,^{12–16} which may be
 86 thermoresponsive.^{17–21}

87 PLA is an approved material by the food and drug
 88 administration (FDA) and used in various implants.^{22–24}
 89 The monomer, lactide, has two asymmetric carbons. PLAs
 90 have different microstructures depending on the configuration
 91 of the monomer. Polymerization of (*S,S*)-lactide (*L*-lactide)
 92 yields isotactic PLLA, while the polymerizations of (*R,S*)-
 93 lactide (*meso*-lactide) or of a racemic mixture of (*R,R*)-lactide
 94 and (*S,S*)-lactide (*DL*-lactide) yield PDLA of irregular
 95 microstructure. PLLA is semicrystalline and less soluble in
 96 organic solvents than the amorphous PDLA.²⁵ PLA in its
 97 various forms has been evaluated for use in injectable drug
 98 delivery formulations,²⁶ especially in the form of nano-
 99 particles.^{27,28} A number of drug delivery studies focused on
 100 micellar structures of diblock copolymers of PLA and poly(2-
 101 ethyl-2-oxazoline) (PEtOx), a lower homologue of PiPOx
 102 approved by the FDA as indirect additive used in food
 103 contacting substances.^{29–31} The calculated solubility parameter
 104 of PEtOx (δ_{PEtOx} : 25.7 J^{0.5}/cm^{1.5}) suggests that PEtOx and
 105 PLA are not miscible. Accordingly, PEtOx-*b*-PLA copolymers
 106 were reported to form core/corona particles. Although PEtOx
 107 is thermoresponsive, the temperature-dependent behavior of
 108 PEtOx-*b*-PLA in water has not been reported.

109 We examine here the self-assembly in water of PiPOx-*b*-PLA
 110 diblock copolymers (Scheme 1). Being aware of the miscibility

Scheme 1. Chemical Structures of PiPOx and the BCPs



exposed to water but confined in close proximity to PLA
 blocks. We demonstrate that the precise particle morphology
 depends on the molecular weight of the PLA and PiPOx blocks
 and on the chirality of the PLA fragment.

EXPERIMENTAL SECTION

Materials. Deionized water (>5 MΩ·cm) or deuterium oxide (D₂O, 99.96% D, Euriso-top) and tetrahydrofuran (THF, >99.9%, inhibitor-free, Honeywell) were used without further purification. Dialysis units (Pur-A-Lyzer, molecular weight cutoff 3500 g/mol, Sigma-Aldrich) were washed in deionized water before use. The diblock copolymers PiPOx-*b*-PLA (Scheme 1 and Table 1, right) were prepared via click coupling of preformed azide-terminated PiPOx with propargyl-terminated PLA using the homopolymers listed in Table 1, left.

Table 1. Molecular Properties of the Polymers Investigated Taken from Ref 3

homopolymers			diblock copolymers			
name ^a	$M_n^{\text{GPC } b}$	PD ^{GPC}	name ^c	$M_n^{\text{NMR } d}$	$\Phi^{\text{PiPOx } e}$	n/m^f
PLLA1	5.9	1.11	2L1	9.5	66	1.9
PLLA2	10.0	1.09	2L2	11.6	50	1.0
PLLA3	14.6	1.06	2L3	14.9	37	0.6
PDLA1	4.9	1.43	2DL1	11.1	53	1.1
PDLA2	9.0	1.41	2DL2	14.3	39	0.6
PDLA3	17.7	1.35	2DL3	19.8	26	0.4
PiPOx2	9.3	1.10	3L1	15.3	74	2.8
PiPOx3	15.5	1.28	3L3	20.2	51	1.0
			3DL1	16.7	65	1.9
			3DL3	25.6	38	0.6

^aNomenclature of homopolymers adopted from ref 3. ^bIn kg/mol, PS calibration, THF as eluent. ^cNomenclature block copolymers: “2L1” = “PiPOx2-*b*-PLLA1”. ^dAbsolute molecular weight in kg/mol, calculated by relating M_n^{MALDI} (PiPOx2:7.1 kg/mol, PiPOx3:12.5 kg/mol) to the ratio of monomeric units obtained from ¹H NMR spectra of the diblocks. ^eIn mol % PiPOx. ^fRatio $n^{\text{PiPOx}}/m^{\text{PLA}}$ of monomeric units in the BCPs as defined in Scheme 1.

Particle Preparation. A PiPOx-*b*-PLA solution in THF (0.5 mL, 132 10 g/L) was added within 1 min to deionized water (2.5 mL) stirred 133 at 300 rpm using a syringe equipped with a needle of 0.4 mm 134 diameter. At the end of the addition, the sample was stirred in air at 135 room temperature for 2 h to remove THF gradually by evaporation. 136 The remaining dispersion was dialyzed against deionized water 137 overnight. The dispersion was recovered and brought to a 138 concentration of 0.5 g/L by addition of deionized water. The 139 dispersion was passed successively through Nuclepore Track-Etched 140 polycarbonate membranes of pore sizes 400, 200, and 100 nm using 141 an Avanti Polar Lipids miniextruder. The dispersion was passed 11 142 times through each membrane. The weight loss of polymer was <5%, 143 as determined gravimetrically. The particles are stable at room 144 temperature for 10 days or longer (see Table S12-1). 145

The same process was used to prepare samples for SANS 146 measurements, starting with a PiPOx-*b*-PLA solution in THF (0.1 147 mL, 50 g/L) and D₂O (0.5 mL). After 1 h of stirring in air, the 148 dispersion was dialyzed against D₂O overnight, brought to a 149 concentration of 5 g/L by addition of D₂O, and extruded as 150 described above. For NMR analysis, dispersions were also prepared in 151 D₂O and brought to a concentration of 25 g/L. They were not 152 extruded. 153

For heat treatment, particle dispersions in H₂O (0.5 g/L) or D₂O 154 (5 g/L) were freshly prepared as described and heated from room 155 temperature to 50 °C at a rate of 1 °C/min. After the temperature was 156 kept at 50 °C for 2 h, the dispersions were cooled back to room 157 temperature at a rate of 1 °C/min and analyzed by light scattering, 158 SANS, or cryo-TEM without further delay. 159

111 of PiPOx and PLA, we designed a comprehensive experimental
 112 approach to determine the morphology of PiPOx-*b*-PLA
 113 particles in aqueous dispersions at 25 °C and upon heating
 114 to 50 °C. ¹H NMR spectroscopy, turbidimetry, high-sensitivity
 115 differential scanning calorimetry (HS-DSC), dynamic light
 116 scattering (DLS), and small-angle neutron scattering (SANS)
 117 led us to conclude that a significant fraction of PiPOx is not

160 **Proton Nuclear Magnetic Resonance Spectroscopy.** ^1H
 161 NMR spectra were recorded with a Bruker Avance III 500
 162 spectrometer. Polymer solutions or dispersions in D_2O were used.
 163 The spectra were recorded at room temperature and normalized to
 164 the intensity of the HOD peak (4.8 ppm).

165 **Light Scattering.** Dynamic (DLS) and static light scattering
 166 (SLS) measurements were performed with a setup consisting of a
 167 Brookhaven Instruments goniometer BIC-200SM, a BIC-TurboCorr
 168 digital auto/cross-correlator, and a BIC-CrossCorr detector combin-
 169 ing two BIC-DS1 detectors. The light source was a Coherent Sapphire
 170 488-100 CDRH laser operating at a wavelength of 488 nm. For details
 171 see the Supporting Information (S-1).

172 **Small-Angle Neutron Scattering.** SANS measurements were
 173 performed at the JEEP II reactor at IFE, Kjeller. The wavelength was
 174 set with the aid of a velocity selector (Dornier), using a wavelength
 175 resolution $\Delta\lambda/\lambda = 10\%$. Two different detector distances (1.0 and 3.4
 176 m) and two wavelengths (5.1 and 10.2 Å) were employed to obtain a
 177 wave-vector range from 0.007 to 0.32 Å $^{-1}$. See the Supporting
 178 Information for details.

179 **Wide-Angle X-ray Scattering.** WAXS measurements were
 180 conducted with a system consisting of a generator (Seifert, 36 kV,
 181 25 mA), a conventional sealed X-ray tube (PANalytical), a Montel
 182 multilayer monochromator, and a 2-dimensional Mar345 image plate
 183 detector (Marresearch GmbH) operating in a perpendicular trans-
 184 mission geometry. The selected wavelength was Cu K α , 1.541 Å.
 185 Dispersions before and after treatment at 50 °C were freeze-dried.
 186 The powders obtained were placed between two Mylar foils separated
 187 with an aluminum ring used as frame.

188 **Transmission Electron Microscopy.** TEM measurements were
 189 performed on a Hitachi FESEM S-4800 electron microscope. Samples
 190 for imaging were prepared by placing a drop of dispersion (0.5 g/L)
 191 on a 300 mesh Cu grid and air-drying. Cryo-TEM observations were
 192 performed with a FEI Talos Arctica microscope operated at 200 kV.
 193 Dispersions (0.5 g/L, 3 μL aliquots) were vitrified with a Leica EMGP
 194 vitrification device using freshly glow-discharged Quantifoil R1.2/1.3
 195 grids. Images were recorded at a 57000 \times magnification with a FEI
 196 Falcon 3 camera operated in the linear mode.

197 **Turbidimetry.** Changes with temperature of the transmittance at
 198 400 nm of a particle dispersion were recorded on a JASCO J-815 CD
 199 spectrometer equipped with a PTC-423S/15 Peltier type temperature
 200 control system. Samples were heated from 20 to 80 °C at a heating
 201 rate of 1 °C/min. The sample temperature was measured via a
 202 thermocouple placed in the dispersion throughout the measurement.

203 **High Sensitivity Differential Scanning Calorimetry.** Thermo-
 204 grams were obtained with a Microcal VP-DSC microcalorimeter.
 205 Degassed dispersions (0.5 g/L) were added to the sample cell (0.52
 206 mL), and measurements were performed at an external pressure of ca.
 207 180 kPa. After an equilibration time of 30 min at 10 °C, the sample
 208 was heated once to 80 °C at a heating rate of 1 °C/min.

209 ■ RESULTS AND DISCUSSION

210 **General Considerations.** The diblock copolymers were
 211 prepared by click ligation of an azide-terminated poly(2-
 212 isopropyl-2-oxazoline) and a propargyl-terminated poly-
 213 (lactide). The molecular characteristics of the homopolymers
 214 PiPOx, PLLA, and PDLLA are presented on the left-hand side
 215 of Table 1. On the right-hand side of Table 1, we give the
 216 composition and molar mass of 10 diblock copolymers
 217 prepared by click coupling of the homopolymers listed on
 218 the left-hand side of Table 1. The PiPOx-*b*-PLAs are organized
 219 in two subsections (entries 1–6 and 7–10) according to the
 220 molecular weight of the PiPOx block. Within each subsection,
 221 the copolymers containing PLLA are listed first, followed by
 222 those containing a PDLLA block. The compositions of four
 223 diblock copolymers studied in detail in this report are printed
 224 in bold font in Table 1. The other samples were used for
 225 specific measurements to identify trends and strengthen the
 226 validity of the mechanisms proposed. We prepared this large

sample set to assess the dependence of the BCPs self-assembly 227
 in water on the BCPs chemical composition, molar mass, and 228
 the lactide chirality. 229

The dispersions were prepared at room temperature by rapid 230
 addition into deionized water of a concentrated solution of the 231
 BCPs in THF, a good solvent for all copolymers. The 232
 copolymers associate in water/THF mixtures of water content 233
 above a given value that depends markedly on the stereo- 234
 chemistry and molecular weight of the PLA block (see Table 235
 S12-1). 236

**^1H NMR Spectroscopy Analysis of Aqueous Copoly- 237
 mer Dispersions at Room Temperature.** In Figure 1, we 238 fi

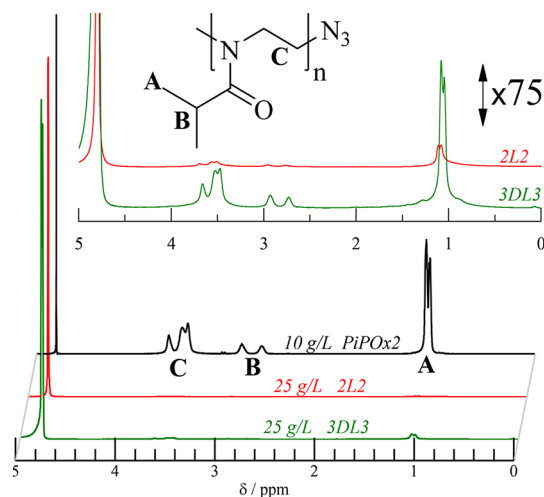


Figure 1. ^1H NMR spectra of dispersions of 2L2 (25 g/L) and 3DL3 (25 g/L) in D_2O . The spectrum (black trace) toward the back of the figure corresponds to a solution of PiPOx2 (10 g/L) in D_2O . Spectra are normalized to the intensity of the HOD signal (δ 4.8 ppm). Intensity-enhanced spectra ($\times 75$) of 2L2 and 3DL3 dispersions are shown in the top section of the figure together with the structure of the PiPOx monomer unit.

present ^1H NMR spectra of PiPOx2 in D_2O (black trace) and 239
 dispersions in D_2O of two PiPOx-*b*-PLA copolymers, 2L2 and 240
 3DL3. The three lower spectra are normalized to the HOD 241
 signal at 4.8 ppm. The ^1H NMR spectrum of PiPOx2 presents 242
 three characteristic signals at ~ 3.5 , 2.8, and 1.1 ppm due to the 243
 resonances of protons C, B, and A (Figure 1). The intensity of 244
 the three signals is reduced significantly in the spectra of 2L2 245
 and 3DL3. On the basis of the nominal concentration of 246
 PiPOx in the copolymer dispersions, we estimate that the 247
 signal around 3.5 ppm ($-\text{CH}_2-\text{CH}_2-\text{N}-$) $_n$ is reduced by 248
 factors of 400 and 150 in the spectra of 2L2 and 3DL3, 249
 respectively, compared to the PiPOx solution. The signals due 250
 to the protons of the hydrophobic PLLA and PDLLA blocks of 251
 2L2 and 3DL3, expected to appear around 5.2 ppm ($-\text{CH}-$) 252
 and 1.6 ppm ($-\text{CH}_3$), cannot be detected at all, which 253
 indicates that the mobility of PLA chains within the 254
 nanoparticles is limited. 255

^1H NMR spectra of typical PLA-containing core-shell 256
 nanoparticles do not present signals due to the PLA blocks, 257
 confined in the core of the micelles. However, they feature 258
 intense signals due to protons of the solvophilic blocks since 259
 they retain their mobility in the corona where they are 260
 surrounded by solvent molecules. The corona block signals 261
 may broaden slightly, but their intensity is hardly affected, as 262
 reported for instance in the case of the related PLA-*b*-PEG 263

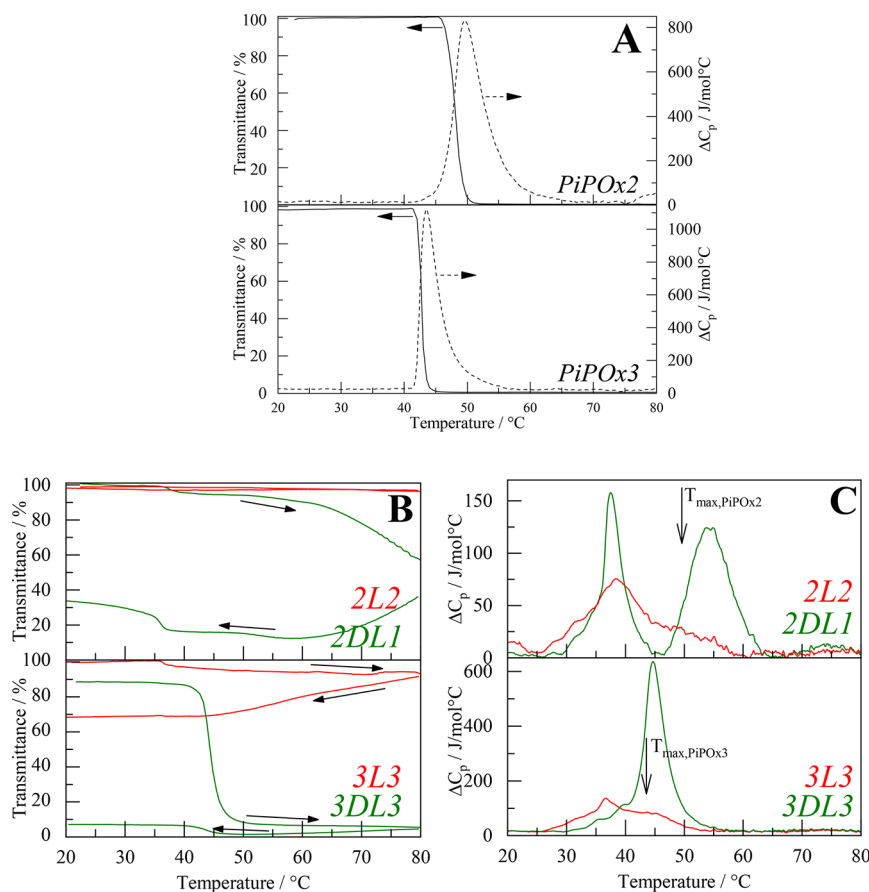


Figure 2. (A) Changes as a function of temperature in the transmittance and heat capacity upon heating of PiPOx2 and PiPOx3 aqueous solutions (polymer concentration: 0.3 g/L). (B) Changes as a function of temperature of the transmittance of 2L2, 2DL1, 3L3, and 3DL3 aqueous dispersions (polymer concentration: 0.5 g/L). The arrows follow the traces recorded upon heating and cooling. (C) Changes with temperature of the heat capacity of 2L2, 2DL1, 3L3, and 3DL3 aqueous dispersions upon heating. Note the difference in the y-scales of the top and bottom panels. The arrows indicate the T_{max} of the corresponding PiPOx solutions (from part A).

Table 2. Thermal Properties of PiPOx Solutions and PiPOx-*b*-PLA Dispersions in Water

	polymer	c_{PiPOx}^a	T_{CP}^b	$T_{\text{max},1}^c$	$T_{\text{max},2}^c$	ΔH_1^d	ΔH_2^d
solutions	PiPOx2	0.30	45.9		49.6		4.8
	PiPOx3	0.30	41.4		43.6		4.8
dispersions	2L2	0.31		38.4	48.8	0.8	
	3L3	0.31		36.6	45.0	1.4	
	2DL1	0.32		37.4	53.5	0.6	0.9
	3DL3	0.25	42.7	39.1	44.7		3.5

^aIn g/L, nominal PiPOx concentration in the solution. ^bIn $^{\circ}$ C, cloud point temperature from turbidimetry. ^cIn $^{\circ}$ C, temperature at the maximum of a transition in HS-DSC. ^dIn kJ/mol, transition enthalpy with an error margin of ± 0.1 kJ/mol.

264 particles dispersed in D₂O.^{34,35} The fact that the PiPOx
 265 protons signals are very weak in the spectra of 2L2 and 3DL3
 266 implies that the PiPOx and PLA chains coexist intermixed via
 267 dipole/dipole interactions through most of the particle volume.
 268 The residual PiPOx signals in the ¹H NMR spectra 2L2 and
 269 3DL3 may be due to residual mobile hydrated PiPOx chains,
 270 presumably located near the water/particle interface.

271 **High-Sensitivity DSC and Turbidimetry.** Four PiPOx-*b*-
 272 PLA dispersions, 2L2, 3L3, 2DL1, and 3DL3, were analyzed by
 273 turbidimetry and microcalorimetry. Solutions of the PiPOx
 274 homopolymers used to prepare the BCPs were evaluated as
 275 well. The BCPs 2L2 and 3L3 differ in terms of their total molar
 276 mass (11.6 kg/mol vs 20.2 kg/mol), but for each BCP the
 277 number of PLA repeat units is nearly the same as the number
 278 of PiPOx units (see Table 1). The BCPs 2DL1 and 3DL3

279 contain DL-lactide. They differ in their total molar mass (11.1
 280 kg/mol vs 25.6 kg/mol) and in the ratio of PiPOx monomer
 281 units to PDLLA repeat units. In all experiments, solutions were
 282 heated from 20 to 80 $^{\circ}$ C (at a rate of 1 $^{\circ}$ C/min) and cooled
 283 back to 20 $^{\circ}$ C with the same rate.

284 **Homopolymer Solutions (Figure 2A and Table 2).** The
 285 cloud points of aqueous PiPOx2 and PiPOx3 solutions
 286 determined by the onset of turbidimetry are 45.9 and 41.4
 287 $^{\circ}$ C, respectively. The corresponding endotherms measured by
 288 HS-DSC are unimodal (Figure 2A, dashed lines). For both
 289 polymers, the onset of the endotherm coincides with the
 290 appearance of turbidity, an indication that the polymers
 291 dehydration is coupled to their aggregation. The enthalpy of
 292 the phase transition (4.8 kJ/mol) is the same for the two
 293 polymers and similar to reported values.⁶ The endotherm is 293

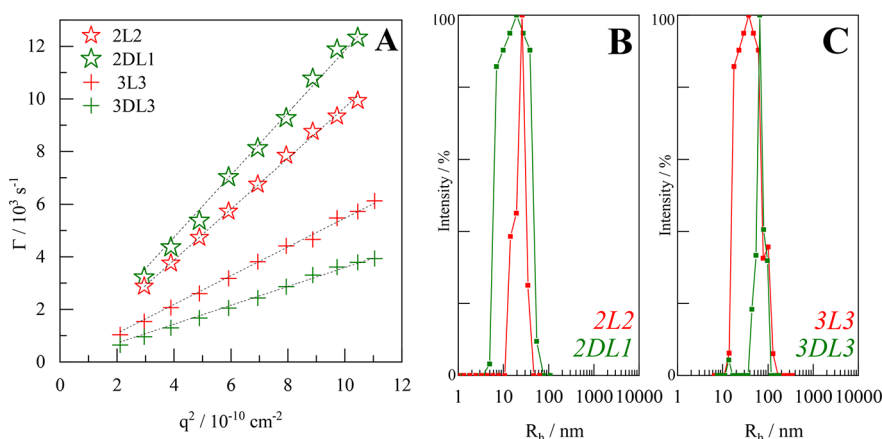


Figure 3. (A) Decay rates Γ from the second-order cumulant analysis vs squared scattering vector q . The dashed lines are linear fits according to $\Gamma = Dq^2$. (B, C) CONTIN plots at scattering angle 90° of the corresponding dispersions.

Table 3. Particle Sizes of PiPOx-*b*-PLA Dispersions Measured by Light Scattering and SANS at 20 °C^a

name	as prepared					after 2 h at 50 °C			
	R_h^b	$\langle \text{Poly} \rangle^c$	R_g^d	R_g/R_h	R^{SANS}	R_h^b	R_g^d	R_g/R_h	R^{SANS}
2L1	19	0.21	20	1.0					
2L2	22	0.17	25	1.1	15.1	24	24	1.0	15.3
2L3	28	0.23	31	1.1					
2DL1	18	0.23	29	1.6	9.9		bimodal		9.2
2DL2	29	0.19	28	0.9					
2DL3	39	0.15	39*	1.0					
3L1	22	0.16	22	1.0					
3L3	39	0.21	42	1.1	17.5^e		bimodal		16.1^d
3DL1	25	0.22	28	1.1					
3DL3	60	0.13	65*	1.1	17.3		bimodal		14.0

^aThe samples were first measured as prepared and second after keeping at 50 °C for 2 h. The bold entries are discussed in the text in more detail. All radii are given in nm. ^bHydrodynamic radius R_h is obtained by the linear fit to the data presented in Figure 3A. ^cAveraged particle dispersity is obtained from second-order cumulant analysis at 11 scattering angles. ^dRadius of gyration R_g is obtained by a fit of first or second order (marked with an asterisk) to the $\ln[P(q)]$ vs q^2 data presented in the Supporting Information. ^eCore-shell model with 12.0 nm core and 5.5 nm shell before heating and 13.3 nm core and 2.8 nm shell after heating.

294 wider in the case of PiPOx2, compared to PiPOx3, which
295 indicates that the cooperativity of the dehydration is less
296 pronounced in the former case.

297 **Dispersions of 3L3 and 2L2 (Figure 2B,C, Red Curves).** The
298 transmittance of the 3L3 dispersion hardly changes over the
299 20–80 °C temperature range: it remains constant (near 100%)
300 up to 36 °C, and then it decreases monotonously with
301 increasing temperature, reaching a value of ~90% at 80 °C. It
302 continues to decrease upon cooling and eventually stabilizes
303 around 70% for $T < 45.0$ °C. The dispersion never recovers its
304 original transmittance, even upon prolonged storage at room
305 temperature (Figure 2B, red traces). The endotherm of the
306 3L3 dispersion is broad, from 25 to 50 °C. It features a weak
307 maximum at 36.6 °C ($T_{\text{max},1}$) and a shoulder at 45.0 °C, a
308 temperature close to the T_{max} of the PiPOx3 solution (Table
309 2). The transition enthalpy, calculated based on the total
310 concentration of iPOx units in solution (2.7 mM), is 1.4 kJ/
311 mol. From this transition enthalpy values, we estimate that
312 ~30% of the PiPOx of the 3L3 dispersion dehydrate upon
313 heating. The HS-DSC and turbidity results are consistent with
314 a 3L3 particle morphology whereby the PiPOx and PLA units
315 of the two blocks form interblock complexes throughout the
316 particles, leaving only a few short tails and loops of PiPOx on
317 the particle outer surface. Short PiPOx oligomer units
318 dehydrate only at high temperature and may remain hydrated

up to 80 °C. The presence of short hydrated PiPOx oligomers 319
may account for the colloidal stability of the 3L3 dispersion up 320
to 80 °C. The small endotherm centered around 36.6 °C is 321
attributed tentatively to the release of water molecules bound 322
to the PiPOx chains confined in the PLA/PiPOx network, by 323
analogy with the dehydration on dense PNIPAM brushes 324
grafted to the surface of gold nanoparticles.³⁶ Such transitions 325
were observed also in the study of starlike micelles formed by 326
hydrophobically end-capped C_{18} -PiPOx-OH (10 kg/mol)³⁷ 327
and attributed to the release of water from dense polymer 328
brushes. 329

The response of 2L2 dispersions to changes in temperature 330
(Figure 2B,C, red lines) is similar to that of 3L3 dispersions. 331
The transition range and $T_{\text{max},1}$ of the two samples are 332
comparable (Table 2). The total enthalpy of the process is 333
lower (0.8 kJ/mol, equivalent to 17% of PiPOx) in the case of 334
2L2 compared to 3L3, and the shoulder on the higher 335
temperature side, centered near T_{max} of the PiPOx2 solution, is 336
less pronounced. The transmittance of 2L2 dispersions hardly 337
changed over the entire heating/cooling scan, which we 338
attribute to the low fraction of PiPOx chains that dehydrate at 339
high temperature (Figure 2B). 340

**Dispersions of 2DL1 and 3DL3 (Figure 2B,C, Green 341
Curves).** The HS-DSC trace of a 2DL1 dispersion exhibits 342
two well-separated endotherms, with $T_{\text{max},1}$ at 37.4 °C (0.6 kJ/ 343

344 mol) and $T_{\max,2}$ at 53.5 °C (0.9 kJ/mol). The total transition
 345 enthalpy is similar to that recorded for a 3L3 dispersion. The
 346 transmittance of a 2DL1 dispersion decreases slightly, from
 347 100 to 95%, around 36.7 °C, remains constant upon heating up
 348 to 52 °C, and decreases to reach a value of ~60% at 80 °C. It
 349 decreases further upon cooling, reaching a minimum (12%) at
 350 60 °C. The transmittance of the dispersion kept at 25 °C
 351 remains constant (34%).

352 The fact that the 3DL3 dispersion remains turbid upon
 353 cooling is surprising. It implies that the 3DL3 aggregation that
 354 occurs at high temperature is not reversible. The thermogram
 355 of the 3DL3 dispersion (Figure 2C, bottom) presents a single
 356 endotherm with $T_m = 44.7$ °C and an enthalpy of 3.5 kJ/mol.
 357 These features indicate that 3DL3 particles prior to heat
 358 treatment adopt a morphology akin to a core/corona
 359 morphology. Given the low enthalpy of the transition, the
 360 core of the particles cannot consist of PLA alone but must
 361 contain complexed PLA and PiPOx blocks.

362 **Light Scattering of Dispersions at Room Temper-**
 363 **ature.** The hydrodynamic size of the BCP particles in aqueous
 364 dispersions at room temperature was determined by DLS.
 365 Autocorrelation functions were analyzed by a second-order
 366 cumulant fit to extract the decay rates Γ between 50° and 150°.
 367 Plots of Γ vs the squared scattering vector q for 2L2, 3L3,
 368 2DL1, and 3DL3 are displayed in Figure 3, together with
 369 CONTIN plots at a scattering angle of 90°. See Figure S3-1 for
 370 Γ vs q^2 plots of the remaining samples. All Γ vs q^2 plots were
 371 linear, which confirms translational diffusion of the nano-
 372 particles. The R_h of the particles increases with the molar mass
 373 of the BCPs, from 18 nm for 2DL1 to 60 nm for 3DL3.

374 The radii of gyration (R_g) (Table 3) of the particles were
 375 obtained by a Guinier fit of the corresponding form factor
 376 functions, $P(\Theta)$, obtained from the average intensity of
 377 scattered light measured by SLS. The dimensionless parameter
 378 $\rho = R_g/R_h$, which reflects the mass distribution of the scattering
 379 object, is an indicator of the morphology of nanoparticles and
 380 of single chain conformation.³⁸ The values of the ρ parameter
 381 vary from 0.9 to 1.1 for all of the BCPs dispersions, except
 382 2DL1 (Table 3). This range of ρ values encompasses 0.926,
 383 the ρ value predicted for collapsed globes, fully permeable to
 384 the solvent and with uniform segment distribution.³⁹ The fact
 385 that the ρ parameter does not change over a wide range of
 386 BCP molecular characteristics is quite remarkable, considering
 387 that the molar fraction of the PiPOx units changes by a factor
 388 of 3 and the solubility properties of PLLA and PDLLA are
 389 entirely different.³⁹ For core/corona particles, such a large
 390 change of the hydrophilic block fraction is accompanied by
 391 significant changes in the extent and density of the corona
 392 detectable through the evolution of the ρ parameter. In the
 393 case of the 2DL1 dispersion, the ρ parameter reaches 1.6. This
 394 point is addressed in relation to SANS data presented in the
 395 following section.

396 **SANS of Dispersions at Room Temperature.** Measure-
 397 ments were carried on dispersions in D₂O of 2L2, 3L3, 2DL1,
 398 and 3DL3.

399 **Dispersions of 2L2 and 3L3 (Figure 4A,B).** The SANS data
 400 collected for the 2L2 dispersion were fitted with a sphere
 401 model of homogeneous density (Figure 4A), yielding a particle
 402 radius, R_{SANS} , of 15.1 nm. A model-independent Guinier fit led
 403 to $R_{g,\text{SANS}} = 14.8$ nm. In the case of the 3L3 dispersion, SANS
 404 data (Figure 4B) were best fitted with a core-shell model,
 405 yielding a particle radius of 17.5 nm and core radius of 12 nm.
 406 The scattering length density (SLD) of the core was initially

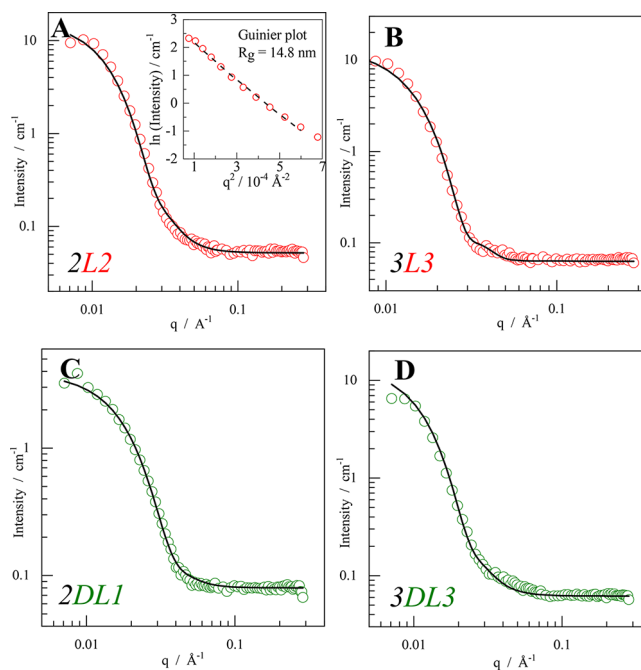


Figure 4. SANS data of the PiPOx-*b*-PLA dispersions (5 g/L, D₂O) directly after preparation measured at 20 °C. The lines are fits to the models described in the text. The inset in (A) shows a Guinier plot.

set to the precalculated value for an averaged PLA/PiPOx
 complex ($1.21 \times 10^{-6} \text{ \AA}^{-2}$). It could be fitted to a value slightly
 higher than that ($1.36 \times 10^{-6} \text{ \AA}^{-2}$), indicating a near-
 homogeneous mixture of PLA and PiPOx in the core with just
 a slight dominance of PLA. However, it should be noted that
 the overall fit is not very sensitive to the core SLD value, so
 that the uncertainty in the value quoted above is relatively large
 (ca. $\pm 0.2 \times 10^{-6} \text{ \AA}^{-2}$). The SANS-derived radii of both 2L2
 and 3L3 are smaller than their hydrodynamic sizes obtained by
 DLS (Table 3). This likely results from the low neutron
 scattering contrast of hydrated regions of the particles, showing
 that the corona is highly diluted and/or not well developed.
 The fact that 2L2 and 3L3 particles appear similar in size in
 SANS indicates that the contrast is lost abruptly at a distance
 from the center of around 15–18 nm. The diffusion-based R_h
 value obtained by DLS is very sensitive to the hydrated
 regions, and the values for the two samples are very different
 (R_h : 22 and 39 nm, respectively). This may indicate that the
 longer PiPOx3 tails extend further in the continuous phase
 than the shorter PiPOx2 chains.

Dispersions of 2DL1 and 3DL3 (Figure 4C,D). 2DL1 is the
 PDLLA analogue to 2L2 in terms of PiPOx mole fraction. The
 SANS data of 2DL1 fitted with a homogeneous sphere model
 yielded $R_{\text{SANS}} = 9.9$ nm (Figure 4C). This low value may
 indicate a high degree of particle hydration, which enhances
 the contrast problem of SANS and is consistent with the much
 higher ρ parameter (1.6) of 2DL1 compared to the other
 samples. The radius of gyration of 2DL1 obtained by light
 scattering is larger by a factor of 2.9 than R_{SANS} (Table 3).
 Thus, both light scattering and SANS argue for a loose and
 highly hydrated PDLLA/PiPOx complex in the 2DL1 particle
 core in comparison to the rather dense PLLA/PiPOx complex
 of 2L2. In the 3DL3 sample the PiPOx mole fraction (38%) is
 lower than in the other examples discussed. The size of 3DL3
 particles derived from SANS data using a homogeneous sphere
 model fit is $R_{\text{SANS}} = 17.3$ nm (Figure 4D). Light scattering of

443 the 3DL3 dispersion yields significantly larger sizes than SANS
 444 (by a factor of 3.8), indicating that the SANS-derived radius is
 445 underestimated due to the low contrast between core and
 446 corona.

447 **Cryo-TEM Observations.** A 3L3 dispersion in water was
 448 vitrified and observed by cryo-TEM. The micrograph (Figure
 449 5) presents diffuse spherical objects of low contrast having an

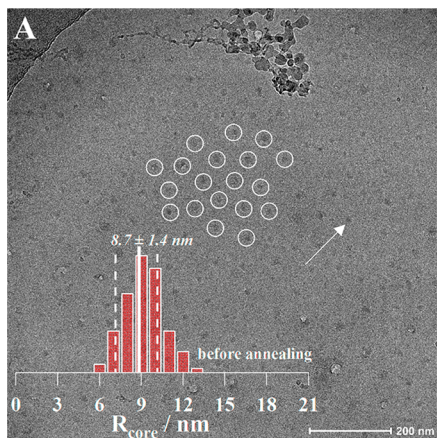


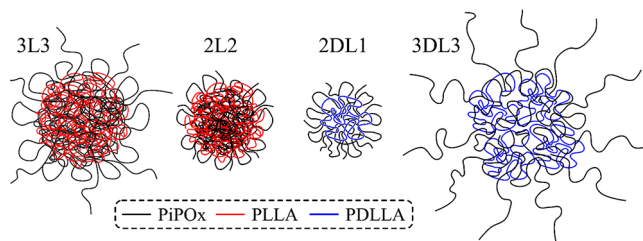
Figure 5. Cryo-TEM image of the 3L3 dispersion vitrified at room temperature immediately after preparation. The inset shows the core radius distribution, and the white circles are a guide for the eye to estimate the particle distance. The arrow points to the core of a particle.

450 average radius of 8.7 ± 1.4 nm, a value smaller than the core
 451 size obtained by SANS (12 nm). Both cryo-TEM and SANS
 452 are sensitive to contrast variations. Cryo-TEM “sees” the
 453 electronic density of the object while the SANS contrast varies
 454 with the hydration level. The spheres are distributed on the
 455 micrograph background at regular intervals, which suggests
 456 that prior to vitrification the dispersed 3L3 particles repelled
 457 each other by steric interactions. The distance between the
 458 centers of contiguous spheres in the micrograph is $\sim 70 \pm 10$
 459 nm, or approximately twice the R_h of the 3L3 particles
 460 determined by DLS (39 nm).

461 **Tentative Morphology of Particles in Aqueous**
 462 **Dispersions at Room Temperature (Scheme 2).** Taken
 463 together the results presented so far indicate that the particles
 464 consist of a core of associated PLA and PiPOx chains held
 465 together via dipole/dipole interactions. The core is surrounded
 466 by tethered hydrated PiPOx chains that extend in the aqueous
 467 continuous phase. The 3L3 particles consist of a dense core, a
 468 hydrated transition region (the shell in the SANS model), and
 469 a corona of PiPOx tails extended into the water phase. The
 470 hydrodynamic sizes of 2L2 and 3L3 are significantly different,
 471 but their ρ parameters are identical, indicating structural
 472 similarities. By SANS, the overall radii of 2L2 and 3L3 are
 473 comparable, but 2L2 is best fitted with a homogeneous sphere
 474 model, whereas in the case of 3L3 a core–shell model gave a
 475 better fit. The more compact, less hydrated, morphology of the
 476 core of the 3L3 particles may reflect the lower solubility of
 477 PLLA3 in water compared to PLLA2. The discrepancy
 478 between the R_{SANS} and R_h reflects differences in the sensitivity
 479 of SANS and DLS toward the outermost parts of the particles.
 480 In conclusion, the corona layer of the 2L2 is comparably thin.
 481 The main difference between the PLLA- and PDLA-
 482 containing particles is the lower density/higher degree of

solvation of the PiPOx/PDLLA complex in the core. This
 results in higher particle elasticity.

Scheme 2. Schematic Illustration of the Particle Structures Formed by 3L3, 2L2, 3DL3, and 2DL1^a



^aFor a detailed description see the text.

Temperature-Dependent Properties of PiPOx-*b*-PLA
Aqueous Dispersions. Turbidity measurements of disper-
 sions of 3L3, 2DL1, and 3DL3 in water (Figure 2B) indicated
 that originally clear dispersions become turbid upon heating
 and remained turbid upon cooling, unlike the dispersion of
 2L2. The high elasticity of the PDLA containing particles and
 the larger extension of the corona layer of the 3L3 particles
 inferred by the SANS data suggest that these particles
 coagulate upon heating. A set of temperature-dependent
 experiments were performed to test this hypothesis. Dis-
 persions of 3L3 (0.5 g/L) were heated from 20 to 51 °C and
 monitored by DLS at 42 °C, i.e., above $T_{max,1}$ but below $T_{max,2}$
 (HS-DSC), and at 51 °C. Subsequently, they were cooled to
 20 °C and tested again. CONTIN plots at a 60° scattering
 angle are displayed in Figure 6. The R_h of the particles initially

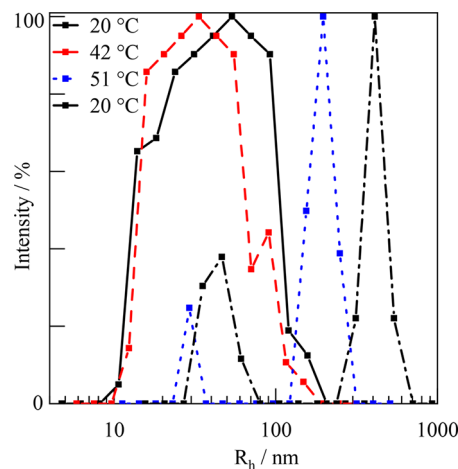


Figure 6. CONTIN plots of 3L3 particles at different temperatures (0.5 g/L, 60° scattering angle). The solid and dash-dotted black lines represent the samples before and after the heating cycle, respectively.

decreases from 49 nm (20 °C) to 40 nm (42 °C). A bimodal
 distribution of particles ($R_h \sim 30$ and 200 nm) is detected at
 51 °C. The dispersion remained bimodal upon cooling to 20
 °C, with distributions of $R_h \sim 45$ and 420 nm. This indicates
 that a fraction of the rehydrated isolated particles is recovered,
 but a significant fraction of the large assemblies formed at 50
 °C do not disassemble upon cooling. It would appear that the
 original particles coagulate into larger objects, which resist
 disintegration upon cooling and rehydration of the PiPOx
 chains. Bimodal distributions were also observed by DLS

510 measurements at 20 °C after keeping the dispersions of 3L3,
511 2DL1, and 3DL3 at 50 °C for 2 h (Table 3 and section S14). In
512 contrast, when the 2L2 dispersion was treated in the same way,
513 no change in the particle size distribution was observed.

514 To determine the morphology of the coagulated particles,
515 freshly prepared 2L2 and 3L3 dispersions were heated to 50 °C
516 and kept at this temperature for 2 h. They were cooled at a rate
517 of 1 °C/min to room temperature and analyzed by SANS,
518 WAXS, and TEM. The SANS data of the 3L3 dispersion
519 (Figure 7A) could not be fitted with a spherical model. Large

about unique properties, highlighted by the remarkable
551 thermal response of the aqueous dispersions: PiPOx-*b*-PLLA
552 dispersions with a short PiPOx block are stable upon heating
553 to 80 °C, a temperature well in excess of the cloud point of
554 PiPOx, with no increase in turbidity; PiPOx-*b*-PDLLA
555 nanoparticles coagulate upon heating and form larger objects
556 of various shapes that do not disintegrate into the pristine
557 nanoparticles upon cooling. 558

We recall that this unique morphology was adopted by over
559 10 PiPOx-*b*-PLA copolymers of different sizes and composi-
560 tions following the identical kinetically controlled experimental
561 protocol: fast addition of a concentrated copolymer solution in
562 tetrahydrofuran into water at room temperature. We currently
563 explore the impact of the preparation method on the
564 nanoparticles morphology and properties. Given the bio-
565 compatibility of PLA and the nontoxicity of PiPOx, one may
566 envisage using PiPOx-*b*-PLA nanoparticles as delivery agents.
567 This raises the interesting question of the ability of PiPOx/
568 PLA mixed phases to accommodate, and release, active agents.
569 The complexation-driven assembly of diblock copolymers
570 offers fundamental challenges and practical opportunities that
571 merit further studies. 572

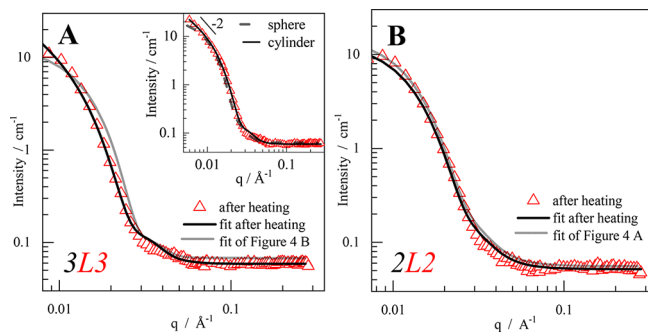


Figure 7. SANS data of the PiPOx-*b*-PLA dispersions (5 g/L, D₂O) after keeping at 50 °C for 2 h, measured at 20 °C. The black lines are fits to the models described in the text, and the gray lines are the respective fits of Figure 4 (pristine particles) for comparison. The inset in (A) compares directly the fits of a sphere and cylinder model for the SANS data after heating, with an indication of the -2 slope at low q values.

520 deviations were observed at low q values (Figure 7A, inset),
521 and a core-shell cylinder model gave a much better fit. The
522 slope of approximately -2 (log-log) at low q values is
523 characteristic of elongated objects with a finite cross section.
524 By use of a cylinder model to characterize these particles, the
525 cross-sectional radius obtained is 16 nm, i.e., just a slight
526 reduction compared to the size of the spheres before heating
527 (17.5 nm). A TEM micrograph of 3L3 particles after heat
528 treatment (Figure S5-1) confirms the presence of large objects
529 of different shapes, including cylindrical objects. In contrast,
530 SANS data of a 2L2 dispersion after heat treatment coincide
531 with those of pristine particles (Figure 7B), confirming that
532 2L2 particles do not coagulate upon heating, in accordance
533 with their more compact morphology deduced from SANS
534 data. WAXS analysis of the 3L3 particles before and after
535 treatment indicated that the PiPOx chains did not crystallize
536 upon heat treatment (see Figure S6-1).

537 CONCLUSIONS

538 Compared to most amphiphilic block copolymers, the
539 assembly of PiPOx-*b*-PLA in water presents distinctive
540 characteristics by virtue of the miscibility of the two blocks
541 in the bulk. Importantly, they do not adopt the typical core-
542 shell morphology whereby the hydrophobic and hydrophilic
543 blocks are segregated respectively in the core and in the shell of
544 a nanoparticle. The core of PiPOx-*b*-PLA nanoparticles
545 dispersed in water consists of associated PiPOx/PLA chains
546 held together by dipole/dipole interactions. Their colloidal
547 stability in water results from the presence of hydrated PiPOx
548 loops and tails at the interface between the core and the
549 aqueous medium. The composition and molar mass of the
550 diblock copolymer subtly modify the morphology, bringing

573 ASSOCIATED CONTENT

574 Supporting Information

The Supporting Information is available free of charge on the
575 ACS Publications website at DOI: 10.1021/acs.macromol.8b02558.
576
577

Solubility of PLA in H₂O/THF mixtures, particle
578 stability at room temperature, detailed light scattering
579 results, TEM of a 3L3 dispersion after heating, and
580 WAXS analysis of freeze-dried 3L3 dispersions (PDF) 581

582 AUTHOR INFORMATION

583 Corresponding Author

*E-mail francoise.winnik@helsinki.fi. 584

585 ORCID

Marjolein Sliepen: 0000-0001-7148-9796 586

Heikki Tenhu: 0000-0001-5957-4541 587

Françoise M. Winnik: 0000-0001-5844-6687 588

589 Notes

The authors declare no competing financial interest. 590

591 ACKNOWLEDGMENTS

This work was supported by Tekes/Finland (Project 1921/31/
592 2012). The use of the facilities and expertise of the CryoEM
593 unit, a member of Biocenter Finland and Instruct-FI, is
594 gratefully acknowledged. F.M.W. acknowledges financial
595 support from the World Premier International Research
596 Center Initiative (WPI), operated by the Ministry of
597 Education, Culture, Sports, Science and Technology
598 (MEXT), Japan, and from the Finnish Distinguished Professor
599 ship grant (TEKES). 600

601 REFERENCES

- 602 (1) Hadjichristidis, N.; Pispas, S.; Floudas, G. *Block Copolymers: Synthetic Strategies, Physical Properties, and Applications*; John Wiley & Sons, Inc.: 2003. 603
- 604 (2) Hebbeker, P.; Steinschulte, A. A.; Schneider, S.; Plamper, F. A. 605 Balancing Segregation and Complexation in Amphiphilic Copolymers 606 by Architecture and Confinement. *Langmuir* 2017, 33 (17), 4091– 607 4106. 608

- 609 (3) Pooch, F.; Sliopen, M.; Svedstrom, K. J.; Korpi, A.; Winnik, F.
610 M.; Tenhu, H. Inversion of Crystallization Rates in Miscible Block
611 Copolymers of Poly(Lactide)-Block-Poly(2-Isopropyl-2-Oxazoline).
612 *Polym. Chem.* **2018**, *9* (14), 1848–1856.
- 613 (4) Fedors, R. F. A Method for Estimating Both the Solubility
614 Parameters and Molar Volumes of Liquids. *Polym. Eng. Sci.* **1974**, *14*
615 (2), 147–154.
- 616 (5) Meyer, M.; Antonietti, M.; Schlaad, H. Unexpected Thermal
617 Characteristics of Aqueous Solutions of Poly(2-Isopropyl-2-Oxazo-
618 line). *Soft Matter* **2007**, *3* (4), 430–431.
- 619 (6) Diab, C.; Akiyama, Y.; Kataoka, K.; Winnik, F. M. Micro-
620 calorimetric Study of the Temperature-Induced Phase Separation in
621 Aqueous Solutions of Poly(2-Isopropyl-2-Oxazolines). *Macromolecules*
622 **2004**, *37* (7), 2556–2562.
- 623 (7) Uyama, H.; Kobayashi, S. A Novel Thermo-Sensitive Polymer.
624 Poly(2-Iso-Propyl-2-Oxazonlie). *Chem. Lett.* **1992**, *21* (9), 1643–
625 1646.
- 626 (8) Zhou, Y.; Tang, H.; Wu, P. Intra-Molecular Interactions
627 Dominating the Dehydration of a Poly(2-Isopropyl-2-Oxazoline)-
628 Based Densely Grafted Polymer Comb in Aqueous Solution and
629 Hysteretic Liquid-Liquid Phase Separation. *Phys. Chem. Chem. Phys.*
630 **2017**, *19* (9), 6626–6635.
- 631 (9) Rudolph, T.; von der Lüh, M.; Hartlieb, M.; Norsic, S.;
632 Schubert, U. S.; Boisson, C.; D'Agosto, F.; Schacher, F. H. Toward
633 Anisotropic Hybrid Materials: Directional Crystallization of Amphi-
634 philic Polyoxazoline-Based Triblock Terpolymers. *ACS Nano* **2015**, *9*
635 (10), 10085–10098.
- 636 (10) Rudolph, T.; Nunns, A.; Stumpf, S.; Pietsch, C.; Schacher, F. H.
637 Hierarchical Self-Assembly of Double-Crystalline Poly-
638 (Ferrocenyldimethylsilane)-Block-Poly(2-Iso-Propyl-2-Oxazoline)
639 (PFDMS-b-PiPrOx) Block Copolymers. *Macromol. Rapid Commun.*
640 **2015**, *36* (18), 1651–1657.
- 641 (11) Park, J.-S.; Akiyama, Y.; Yamasaki, Y.; Kataoka, K. Preparation
642 and Characterization of Polyion Complex Micelles with a Novel
643 Thermosensitive Poly(2-Isopropyl-2-Oxazoline) Shell via the Com-
644 plexation of Oppositely Charged Block Ionomers. *Langmuir* **2007**, *23*
645 (1), 138–146.
- 646 (12) Korchagina, E. V.; Qiu, X.-P.; Winnik, F. M. Effect of Heating
647 Rate on the Pathway for Vesicle Formation in Salt-Free Aqueous
648 Solutions of Thermosensitive Cationic Diblock Copolymers. *Macro-*
649 *molecules* **2013**, *46* (6), 2341–2351.
- 650 (13) An, J.; Liu, X.; Dedinaite, A.; Korchagina, E.; Winnik, F. M.;
651 Claesson, P. M. Effect of Solvent Quality and Chain Density on
652 Normal and Frictional Forces between Electrostatically Anchored
653 Thermoresponsive Diblock Copolymer Layers. *J. Colloid Interface Sci.*
654 **2017**, *487*, 88–96.
- 655 (14) Zschoche, S.; Rueda, J. C.; Binner, M.; Komber, H.; Janke, A.;
656 Appelhans, D.; Voit, B. Temperature- and PH-Dependent Aggrega-
657 tion Behavior of Hydrophilic Dual-Sensitive Poly(2-Oxazoline)s
658 Block Copolymers as Latent Amphiphilic Macromolecules. *Eur.*
659 *Polym. J.* **2017**, *88*, 623–635.
- 660 (15) Legros, C.; De Pauw-Gillet, M.-C.; Tam, K. C.; Taton, D.;
661 Lecommandoux, S. Crystallisation-Driven Self-Assembly of Poly(2-
662 Isopropyl-2-Oxazoline)-Block-Poly(2-Methyl-2-Oxazoline) above the
663 LCST. *Soft Matter* **2015**, *11* (17), 3354–3359.
- 664 (16) An, J.; Dédinaite, A.; Winnik, F. M.; Qiu, X.-P.; Claesson, P. M.
665 Temperature-Dependent Adsorption and Adsorption Hysteresis of a
666 Thermoresponsive Diblock Copolymer. *Langmuir* **2014**, *30* (15),
667 4333–4341.
- 668 (17) Takahashi, R.; Qiu, X.-P.; Xue, N.; Sato, T.; Terao, K.; Winnik,
669 F. M. Self-Association of the Thermosensitive Block Copolymer
670 Poly(2-Isopropyl-2-Oxazoline)-b-Poly(N-Isopropylacrylamide) in
671 Water–Methanol Mixtures. *Macromolecules* **2014**, *47* (19), 6900–
672 6910.
- 673 (18) Takahashi, R.; Sato, T.; Terao, K.; Qiu, X.-P.; Winnik, F. M.
674 Self-Association of a Thermosensitive Poly(Alkyl-2-Oxazoline) Block
675 Copolymer in Aqueous Solution. *Macromolecules* **2012**, *45* (15),
676 6111–6119.
- (19) Salzinger, S.; Huber, S.; Jaksch, S.; Busch, P.; Jordan, R.; 677
Papadakis, C. M. Aggregation Behavior of Thermo-Responsive 678
Poly(2-Oxazoline)s at the Cloud Point Investigated by FCS and 679
SANS. *Colloid Polym. Sci.* **2012**, *290* (5), 385–400. 680
- (20) Zhou, Y.; Wu, P. Block Length-Dependent Phase Transition of 681
Poly(N-Isopropylacrylamide)-b-Poly(2-Isopropyl-2-Oxazoline) Di- 682
block Copolymer in Water. *Polymer* **2018**, *153*, 250–261. 683
- (21) Kondo, M.; Takahashi, R.; Qiu, X.-P.; Winnik, F. M.; Terao, K.; 684
Sato, T. Small-Angle X-Ray Scattering from the Concentrated Bulk 685
Phase Separated from an Amphiphilic Block-Copolymer Solution. 686
Polym. J. **2017**, *49*, 385. 687
- (22) Saini, P.; Arora, M.; Kumar, M. N. V. R. Poly(Lactic Acid) 688
Blends in Biomedical Applications. *Adv. Drug Delivery Rev.* **2016**, *107*,
47–59. 689
- (23) Santoro, M.; Shah, S. R.; Walker, J. L.; Mikos, A. G. Poly(Lactic 691
Acid) Nanofibrous Scaffolds for Tissue Engineering. *Adv. Drug* 692
Delivery Rev. **2016**, *107*, 206. 693
- (24) Tyler, B.; Gullotti, D.; Mangraviti, A.; Utsuki, T.; Brem, H. 694
Polylactic Acid (PLA) Controlled Delivery Carriers for Biomedical 695
Applications. *Adv. Drug Delivery Rev.* **2016**, *107*, 163–175. 696
- (25) Pretula, J.; Slomkowski, S.; Penczek, S. Poly lactides—Methods 697
of Synthesis and Characterization. *Adv. Drug Delivery Rev.* **2016**, *107*,
3. 698
699
- (26) Jain, A.; Kunduru, K. R.; Basu, A.; Mizrahi, B.; Domb, A. J.; 700
Khan, W. Injectable Formulations of Poly(Lactic Acid) and Its 701
Copolymers in Clinical Use. *Adv. Drug Delivery Rev.* **2016**, *107*, 213–
227. 702
703
- (27) Nicolas, J.; Mura, S.; Brambilla, D.; Mackiewicz, N.; Couvreur, 704
P. Design, Functionalization Strategies and Biomedical Applications 705
of Targeted Biodegradable/Biocompatible Polymer-Based Nano- 706
carriers for Drug Delivery. *Chem. Soc. Rev.* **2013**, *42* (3), 1147–1235. 707
- (28) Lee, B. K.; Yun, Y.; Park, K. PLA Micro- and Nano-Particles. 708
Adv. Drug Delivery Rev. **2016**, *107*, 176. 709
- (29) Hsiue, G.-H.; Wang, C.-H.; Lo, C.-L.; Wang, C.-H.; Li, J.-P.; 710
Yang, J.-L. Environmental-Sensitive Micelles Based on Poly(2-Ethyl-2- 711
Oxazoline)-b-Poly(L-Lactide) Diblock Copolymer for Application in 712
Drug Delivery. *Int. J. Pharm.* **2006**, *317* (1), 69–75. 713
- (30) Shieh, M.-J.; Peng, C.-L.; Chiang, W.-L.; Wang, C.-H.; Hsu, C.- 714
Y.; Wang, S.-J. J.; Lai, P.-S. Reduced Skin Photosensitivity with Meta- 715
Tetra(Hydroxyphenyl)Chlorin-Loaded Micelles Based on a Poly(2- 716
Ethyl-2-Oxazoline)-b-Poly(d,l-Lactide) Diblock Copolymer in Vivo. 717
Mol. Pharmaceutics **2010**, *7* (4), 1244–1253. 718
- (31) Lee, S. C.; Chang, Y.; Yoon, J.-S.; Kim, C.; Kwon, I. C.; Kim, 719
Y.-H.; Jeong, S. Y. Synthesis and Micellar Characterization of 720
Amphiphilic Diblock Copolymers Based on Poly(2-Ethyl-2-Oxazo- 721
line) and Aliphatic Polyesters I. *Macromolecules* **1999**, *32* (6), 1847–
1852. 722
723
- (32) Schärfl, W. *Light Scattering from Polymer Solutions and* 724
Nanoparticle Dispersions; Springer: Berlin, 2007. 725
- (33) Agrawal, S. K.; Sanabria-DeLong, N.; Tew, G. N.; Bhatia, S. R. 726
Structural Characterization of PLA-PEO-PLA Solutions and 727
Hydrogels: Crystalline vs Amorphous PLA Domains. *Macromolecules* 728
2008, *41* (5), 1774–1784. 729
- (34) Heald, C. R.; Stolnik, S.; Kujawinski, K. S.; De Matteis, C.; 730
Garnett, M. C.; Illum, L.; Davis, S. S.; Purkiss, S. C.; Barlow, R. J.; 731
Gellert, P. R. Poly(Lactic Acid)-Poly(Ethylene Oxide) (PLA-PEG) 732
Nanoparticles: NMR Studies of the Central Solidlike PLA Core and 733
the Liquid PEG Corona. *Langmuir* **2002**, *18* (9), 3669–3675. 734
- (35) Pagels, R. F.; Edelstein, J.; Tang, C.; Prud'homme, R. K. 735
Controlling and Predicting Nanoparticle Formation by Block 736
Copolymer Directed Rapid Precipitations. *Nano Lett.* **2018**, *18* (2),
1139–1144. 737
738
- (36) Shan, J.; Chen, J.; Nuopponen, M.; Tenhu, H. Two Phase 739
Transitions of Poly(N-Isopropylacrylamide) Brushes Bound to Gold 740
Nanoparticles. *Langmuir* **2004**, *20* (11), 4671–4676. 741
- (37) Obeid, R.; Tanaka, F.; Winnik, F. M. Heat-Induced Phase 742
Transition and Crystallization of Hydrophobically End-Capped 743
Poly(2-Isopropyl-2-Oxazoline)s in Water. *Macromolecules* **2009**, *42*
744
745

- 746 (38) Mössmer, S.; Spatz, J. P.; Möller, M.; Aberle, T.; Schmidt, J.;
747 Burchard, W. Solution Behavior of Poly(Styrene)-Block-Poly(2-
748 Vinylpyridine) Micelles Containing Gold Nanoparticles. *Macro-*
749 *molecules* **2000**, 33 (13), 4791–4798.
- 750 (39) Allegra, G.; Ganazzoli, F. Polymer Collapse in Dilute Solution:
751 Equilibrium and Dynamical Aspects. *J. Chem. Phys.* **1985**, 83 (1),
752 397–412.